UCLA
UCLA Previously Published Works

Title

Microengineered 3D cell-laden thermoresponsive hydrogels for mimicking cell morphology and orientation in cartilage tissue engineering

Permalink

Journal

ISSN

Authors

Mellati, Amir
Fan, Chia-Ming
Tamayol, Ali
et al.

Publication Date

2017

DOI

Microengineered 3D Cell-Laden Thermoresponsive Hydrogels for Mimicking Cell Morphology and Orientation in Cartilage Tissue Engineering

Amir Mellati,[1] Chia-Ming Fan,[2] Ali Tamayol,[3,4,5] Nasim Annabi,[3,4,5,6] Sheng Dai,[1] Jingxiu Bi,[1] Bo Jin,[1] Cory Xian,[2] Ali Khademhosseini,[3,4,5,7] Hu Zhang[1]

[1]School of Chemical Engineering, The University of Adelaide, Adelaide, SA 5005, Australia; telephone: + 61 8 8313 3810; fax: +61 8 8313 4373; e-mail: hu.zhang@adelaide.edu.au

[2]School of Pharmacy and Medical Sciences, Sansom Institute for Health Research, University of South Australia, Adelaide, SA, Australia

[3]Biomaterials Innovation Research Center, Division of Biomedical Engineering, Department of Medicine, Brigham and Women's Hospital, Harvard Medical School, Boston, Massachusetts 02139; telephone: +1 617 768 8395; fax: +1 617 768 8477; e-mail: alik@rics.bwh.harvard.edu

[4]Harvard-Massachusetts Institute of Technology Division of Health Sciences and Technology, Massachusetts Institute of Technology, Cambridge, Massachusetts 02139

[5]Wyss Institute for Biologically Inspired Engineering, Harvard University, Boston, Massachusetts 02115

[6]Department of Chemical Engineering, Northeastern University, Boston, Massachusetts

[7]Department of Bioindustrial Technologies, College of Animal Bioscience and Technology, Konkuk University, Hwayang-dong, Gwangjin-gu, Seoul 143-701, Republic of Korea

ABSTRACT: Mimicking the zonal organization of native articular cartilage, which is essential for proper tissue functions, has remained a challenge. In this study, a thermoresponsive copolymer of chitosan-g-poly(N-isopropylacrylamide) (CS-g-PNIPAAm) was synthesized as a carrier of mesenchymal stem cells (MSCs) to provide a support for their proliferation and differentiation. Microengineered three-dimensional (3D) cell-laden CS-g-PNI-PAAm hydrogels with different microstripe widths were fabricated to control cellular alignment and elongation in order to mimic the superficial zone of natural cartilage. Biochemical assays showed six- and sevenfold increment in secretion of glycosaminoglycans (GAGs) and total collagen from MSCs encapsulated within the synthesized hydrogel after 28 days incubation in chondrogenic medium. Chondrogenic differentiation was also verified qualitatively by histological and immunohistochemical assessments. It was found that $75 \pm 6\%$ of cells encapsulated within $50\,\mu m$ wide microstripes were aligned with an aspect ratio of 2.07 ± 0.16 at day

5, which was more organized than those observed in unpatterned constructs ($12 \pm 7\%$ alignment and a shape index of 1.20 ± 0.07). The microengineered constructs mimicked the cell shape and organization in the superficial zone of cartilage whiles the unpatterned one resembled the middle zone. Our results suggest that microfabrication of 3D cell-laden thermosensitive hydrogels is a promising platform for creating biomimetic structures leading to more successful multi-zonal cartilage tissue engineering.

Introduction

Cartilage-related diseases such as arthritis are among the most common reasons for giving rise to disabilities around the world (Keeney et al., 2011). Daily accidents are another major cause of cartilage damage. Articular cartilage covers the bone heads in articulating joints and facilitates the smooth motion of joints (Mansour, 2003). This multiphasic tissue consists of chondrocyte cells, interstitial fluid, and extracellular matrix (ECM). Collagen fibers and proteoglycans (PG) are the main components of ECM (Newman, 1998). Three main zones are distinguishable in articular
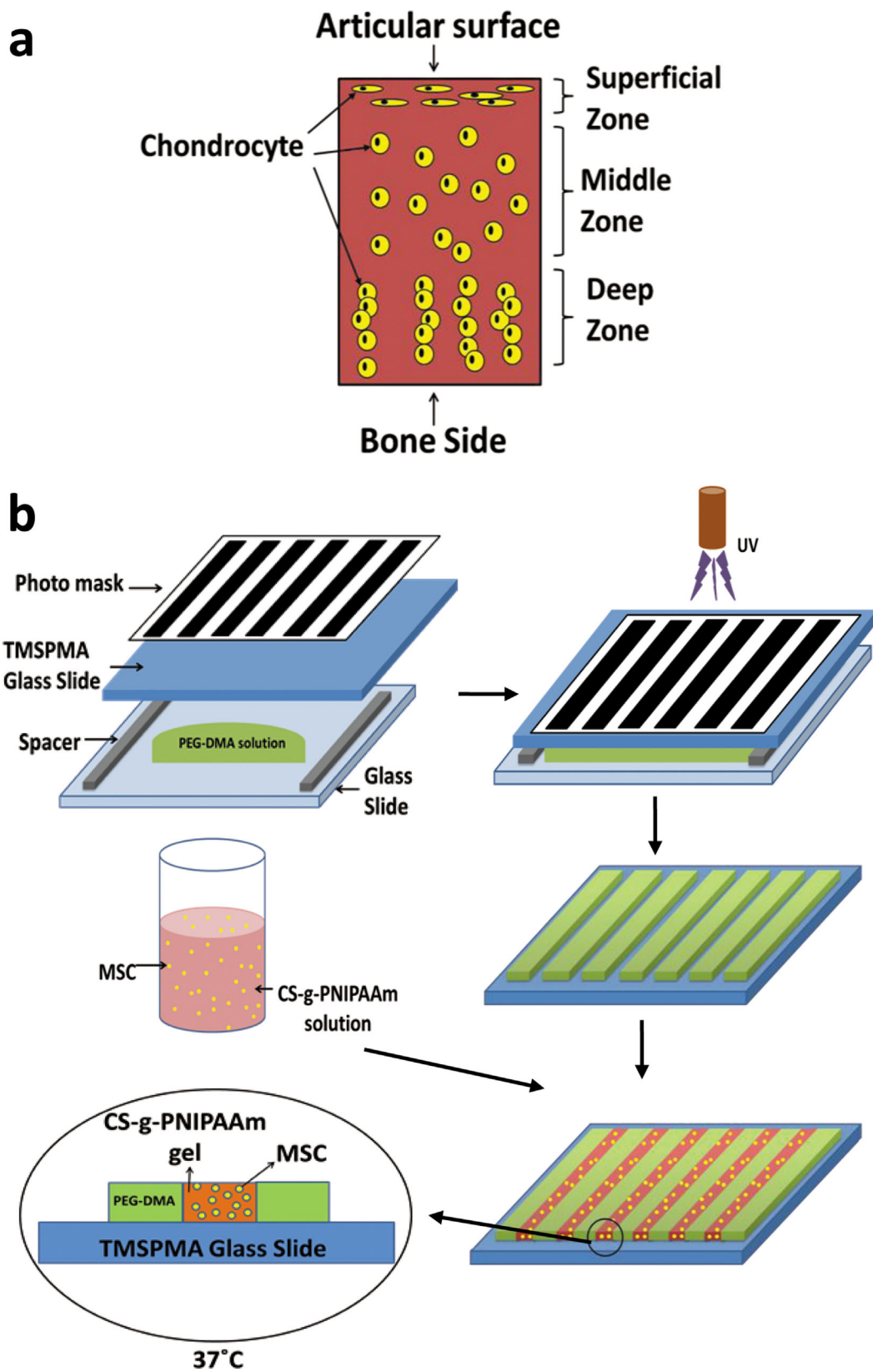
Scheme 1. (a) Cell alignment and elongation within different zones of native articular cartilage. (b) Schematic diagram illustrating the fabrication of the micropatterned cell-laden hydrogels. PEG-DMA micromolds are made using photolithography. CS-g-PNIPAAm solution including MSCs is thermally casted whithin the micromold channels to form microengineered 3D cell-laden hydrogels at 37 °C.

cartilage as shown in Scheme 1a (Temenoff and Mikos, 2000). The closest layer to the cartilage surface is called superficial zone where chondrocytes are ellipsoidal and parallel to the surface. The middle or transitional zone is located under the superficial zone and the chondrocytes of this region are randomly aligned and less elongated. The deep zone is below the middle layer and chondrocytes are spherical and aligned columnar to the tidemark (Hunziker et al., 2002; Poole et al., 2001; Wise et al., 2008). The mechanical properties and biochemical compositions of each layer are different from others.

Articular cartilage has limited self-repair capacity, thus developing treatment strategies that can restore its function are highly important (Hunziker, 2002). Tissue engineering has emerged as a promising solution for treating damaged articular cartilage. However, many challenges remain to be addressed for engineering functional cartilage, including selecting an appropriate cell source and a matrix for hosting the cells to support their proliferation and tissue remodeling. Another key challenge is recreation of the zonal organization observed in the native articular cartilage. Among various cell sources proposed for cartilage tissue engineering, mesenchymal stem cells (MSCs) are considered as an attractive candidate because of their ease of isolation, capability for in vitro expansion, and controllable differentiation into cartilage (Johnstone et al., 2013; Lanza et al., 2007). In addition, it has been shown that MSCs can be differentiated to zonal chondrocytes in a suitable microenvironment (Coates and Fisher, 2014). Among various matrices explored for cartilage tissue engineering, hydrogels have drawn significant attention due to their similarity to the natural ECM of the cartilage as a highly hydrated tissue (Spiller et al., 2011). Chitosan-based hydrogels possess a molecular structure similar to glycosaminoglycans (GAGs) and hyaluronic acid in PGs of native articular cartilages. Thus, they have shown great potential to enhance chondrogenesis and to modulate the cell proliferation, differentiation, and function (Di Martino et al., 2005; Fedorovich et al., 2007; Francis Suh and Matthew, 2000; Kim et al., 2008).

Recreating the spatial organization of native articular cartilage, which is expected to play an important role in function of engineered tissues, has stayed an unmet challenge. This complex zonal organization supports cartilage functions within body joints (McCullen et al., 2012). Various strategies including cell-, matrix-, bioreactor-, and bioactive molecule-based approaches have been employed to mimic the layered structure of the native articular cartilage. Some of these strategies have been focused on regenerating the zone-specific ECM biochemical compositions at a molecular level, or on mimicking the zone-specific mechanical properties. Efforts have also been made in resembling the layered physical microarchitecture of the native cartilage, such as controlling cellular morphology and arrangement. In cell-based approaches, the incorporation of different zonal chondrocytes in a depth-dependent fashion within either a single layer (Klein et al., 2003) or multilayered hydrogel of the same material (Kim et al., 2003; Sharma et al., 2007) was found to have a potential to recreate biomimetic zones. Matrices have also been manipulated to recapitulate the organized zonal architecture of the native cartilage. Encapsulation of MSCs (Nguyen et al., 2011; Sharma and Elisseeff, 2004) or chondrocytes (Klein et al., 2010; Lee et al., 2007; Walker and Madihally, 2014) in multilayered

constructs formed from a single or multiple hydrogels have shown encouraging results. Other matrix-based strategies include spatially varying the physical and mechanical properties by altering gel concentration (Ng et al., 2005), degradability (Bryant and Anseth, 2003), pore size through bioprinting (Woodfield et al., 2005), nanofiber size and orientation (McCullen et al., 2012; Wise et al., 2008), nanoparticle concentration (Erisken et al., 2008), and combinatorial scaffold morphologies (e.g., electrospun poly(caprolactone) [PCL] fibers on top and porous PCL scaffold in bottom) (Steele et al., 2014). Although all of these approaches have shown promising results, they are complicated and required multiple step fabrication. Another alternative approach for tuning the spatial cellular behavior is to create gradient of mechanical and chemical cues using a bioreactor (Chen et al., 2013; Kock et al., 2013; Marsano et al., 2006; Spitters et al., 2013). Gradient delivery of bioactive molecules or nutrients such as oxygen (Schrobback et al., 2012) and glucose (Spitters et al., 2014) has also been attempted. Perhaps, the combination of various approaches may enhance the zonal variation similar to the inhomogeneity of the native cartilage but it may add more complexity to the system, which make the optimization process more challenging (Hwang et al., 2007b; Thorpe et al., 2013).

Recent advances in synthesis of photocrosslinkable hydrogels combined with the developments of photolithography techniques have enabled the fabrication of finely tuned constructs with precise control on the spatial distribution of physical and chemical cues (Annabi et al., 2014). It has been demonstrated that micropatterning is an effective method for controlling cellular alignment and elongation in 2D and 3D (Nichol et al., 2010). In this study, we aim to use photolithography for creating 3D patterned microconstructs to control cellular orientation and mimic the zonal organization observed in native cartilage tissues. However, a key concern associated with the use of UV irradiation for the crosslinking of cell-laden hydrogel constructs is the cell and DNA damage by UV or UV-induced free radicals (Albrecht et al., 2005; Liu and Bhatia, 2002). For example, cell viability is highly dependent on UV exposure time and photoinitiator concentration (Liu and Bhatia, 2002), which are critical parameters in regulation of hydrogel physical and mechanical properties as well. As a consequence, preparation of such constructs with optimum properties might reduce cellular viability. On the other hand, thermoresponsive polymers whose solution becomes gel at a physiological temperature have gained great interest in recent years. The influences of these hydrogels on regulating cell responses have been studied by many groups, for example, osteogenic (Ren et al., 2015), chondrogenic (Cho et al., 2004), and myogenic (Xu et al., 2015) differentiation of MSCs.

We synthesized a thermoresponsive hydrogel based on chitosan-g-poly(N-isopropylacrylamide) (CS-g-PNIPAAm) and evaluated its suitability for chondrogenic differentiation of MSCs as well as their alignment in the microfabricated 3D hydrogels. Micromolds based on poly (ethylene glycol)-dimethacrylate (PEG-DMA) were created and the MSC-laden copolymer was then thermally cast into the PEG-DMA micromolds to form cell-laden micropatterned hydrogel, which mimic the cell shape and orientation in superficial zone of native articular cartilage. Our results suggest that the micro-engineered 3D cell-laden CS-g-PNIPAAm can offer great promise in engineering bi-zonal cartilage.

Materials and Methods

CS-g-PNIPAAm Synthesis and Characterization

CS-g-PNIPAAm was synthesized by free radical grafting polymerization as described in our recent work (Mellati et al., 2014). Briefly, N-isopropylacrylamide (NIPAAm) (Sigma–Aldrich, Castle Hill, Australia) was purified by recrystallization in n-hexane, and then 1 wt% chitosan (MW of 200–300 kDa) (Acros Organic, Morris, NJ) in 30 mL aqueous acetic acid (10 wt%) was mixed with 17.7 mmol purified NIPAAm monomer and the mixture was degassed. Polymerization was initiated by adding 0.18 mmol ammonium cerium (IV) nitrate (CAN) (Acros Organic) and reaction was carried out for 24 h under nitrogen atmosphere. The solution was condensed and precipitated in an excess amount of tetrahydrofuran/hexane (4:1). The precipitate was further purified by methanol soxhlet extraction for 48 h. The purified product was dried under vacuum. Two products (CS-NI-1 and CS-NI-2) with different properties were obtained at the polymerization temperature of 60 and 25 °C, respectively. Rheological measurements were conducted using a SR5 controlled stress rheometer (Rheometric Scientific, Piscataway, NJ) as described elsewhere (Mellati et al., 2014). Storage modulus was read at 1 rad/s and 37 °C for 3.0 wt% of CS-g-PNIPAAm copolymers in PBS (pH = 7.4). Grafting ratio (GR) was calculated as $(W_2 - W_1)/W_1 \times 100\%$, where W_1 and W_2 are the weights of initial chitosan loaded and PNIPAAm-grafted chitosan after soxhlet extraction, respectively.

3D Cell Encapsulation

MSCs (murine, 10T1/2, RIKEN cell bank, Japan) were cultured in Dulbecco's modified Eagle's Medium (DMEM) supplemented with 10% fetal bovine serum (FBS), 100 U/mL of penicillin, 100 mg/mL of streptomycin, and 2 mM/L L-glutamine (All from Gibco, Grand Island, NY) and incubated at 37 °C in a humidified atmosphere with 5% CO_2. MSCs were trypsinized and resuspended in a fresh growth medium for further use.

In a typical 3D cell encapsulation experiment, the polymer was dissolved in PBS (pH of 7.4) at the concentration of 31.5 mg/mL and was autoclaved prior to use. Cell suspension and copolymer solution were mixed. The final cell and polymer concentration were 1.0×10^6 cells/mL and 3.0 wt%, respectively. Cell-laden hydrogels were prepared by adding 300 μL of the cell/polymer mixture to each well on a 24-well plate and 1 h incubation at 37 °C. Cells and PBS without copolymer were also mixed to prepare negative control at the same cell density. Fresh growth medium (2 mL) was added to the top of each well and further incubated in an incubator at 37 °C and 5% CO_2 for 7 days. Medium was replaced with fresh medium once every other day. CS-NI-1 and CS-NI-2 hydrogel samples were used to compare the cell performance and the best sample was further employed for investigating the influence of polymer concentration on cell proliferation. The same procedure was repeated using 2.0, 2.5, and 3.0 wt% solutions of the selected polymer sample.

MTT Assay

Cell viability and proliferation of the cell-encapsulated hydrogels were evaluated using the MTT assay. At each time point, 0.5 mL of 3-(4,5-dimethylthiazol-2-yl)-2,5-diphenyltetrazolium bromide (MTT) (Molecular Probes, Eugene, OR) (5 mg/mL in PBS) was added to each well. After incubation for 4 h at 37 °C, all the liquid content was replaced with 1 mL dimethyl sulfoxide (DMSO) and further kept in the incubator to solubilize formazan crystals. All well content (including liquid and gel) was transferred to an eppendorf tube, vortexed briefly, and centrifuged at 10,000 rpm for 5 min. Finally, 200 μL of supernatant was transferred to a 96-well plate and the absorbance was read using a microplate reader (ELx808, BioTek, Winooski, VT) at 595 nm. The absorbance of cell-free hydrogels (negative control) incubated with MTT solution was deducted from cell-encapsulated hydrogels to remove any interference from hydrogel-MTT reaction. The results are the mean of measured values for three independent samples.

MSC Differentiation in 3D Hydrogel

The selected polymer from the previous experiments was mixed with MSC suspension so that the final cell density was 1.0×10^7 cells/mL of hydrogel and the final polymer concentration was fixed at the optimized value obtained from the above experiment. Transferable wells were prepared by mounting Press-To-Seal^{TM} silicone rubbers (Molecular Probes) on cover glasses and the wells were then sterilized. The cell-polymer solution (300 μL) was added to the wells and incubated at 37 °C until the cell-embedded hydrogels were formed. Rubber-made wells were transferred to a 6-well plate. Five milliliter of chondrogenic medium was added to each well, containing high glucose-DMEM, 1% insulin, transferrin, selenous acid (ITS) + Permix (BD Bioscience, Sparks, MD), 10^{-7} M dexamethasone (Sigma–Aldrich), 10 ng/mL transforming growth factor-beta 1 (TGF-β1) (Peprotech, Rocky Hill, NJ), 50 μg/mL ascorbate-2-phosphate (Sigma–Aldrich), 100 U/mL of penicillin, 100 mg/mL of streptomycin, and 2 mM/L L-glutamine. Constructs were kept in incubator at 37 °C and 5% CO_2 for 28 days. The media was refreshed every day.

Biochemical Analysis

DNA, GAG, and total collagen content were quantified by Hoechst 33258, (1,9-dimethylmethylene blue) (DMMB), and hydroxyproline assays as described previously (Hoemann, 2004; Hwang et al., 2007a). At each time point, constructs were collected, rinsed with pre-warmed PBS, freeze-dried for 48 h and digested by incubation in a papain (Sigma–Aldrich) solution (125 μg/mL) at 60 °C for 16 h. The supernatant of the papain-digested hydrogels was used for biochemical assessment.

DNA content was measured by the Hoechst 33258 assay. A 30 μL of the supernatant of the papain-digested constructs was added to 3 mL of 0.1 μg/mL Hoechst 33258 dye (Sigma–Aldrich) solution in TNE buffer (10 mM Tris–HCl, 100 mM NaCl, 1 mM EDTA) and the intensity was read using a RF-5301PC fluorospectrometer (Shimadzu, Kyoto, Japan) at 360 nm excitation and 460 nm emission. The corresponding DNA amount was calculated based on a ds-calf Thymus DNA type I (Sigma–Aldrich) standard curve.

For GAG analysis, the supernatant was reacted with DMMB (Sigma–Aldrich) in PBE buffer (100 mM phosphate buffer, 10 mM EDTA) solution (46 μM) and absorbance was read at 525 nm by the

spectrophotometer. Chondroitin sulphate (Sigma–Aldrich) was served to generate a standard curve.

Total collagen was evaluated by the hydroxyproline assay. Papain-digested supernatant was hydrolyzed in 6 N HCl for 18 h at 110 °C, then neutralized and combined with chloramine-T (Sigma–Aldrich) solution (15.7 mg/mL) followed by incubation at room temperature for 20 min. The solution was mixed with Ehrlich's reagent, vortexed and further incubated for 30 min at 60 °C. Finally, the absorbance was read at 550 nm using the spectrophotometer and collagen content was computed according to the trans-4-hydroxy-L-proline (Sigma–Aldrich) standard curve. All values of biochemical assays were normalized to the dry weight of the constructs.

Histological and Immunohistochemical Staining

Cell-seeded hydrogels were transferred into cryomolds, embedded in Tissue-Tek® O.C.T™ compound (Sakura, Alphen aan den Rijn, the Netherlands), and then cryosectioned in 10 μm thickness. Sections were fixed in cold acetone for 10 min, air dried and washed in PBS. Cell-laden microconstructs were also fixed in 4% paraformaldehyde for 30 min. For GAG histological staining, sections were stained in 1% safranin O (Sigma–Aldrich) solution for 30 min. Immunohisto-chemical staining was also used to identify collagen type II (a commonly used marker for chondrogenesis) (Chung et al., 2006). Sections were quenched in 3% hydrogen peroxide for 20 min and treated with 1.0 μg/mL proteinase K for 20 min for antigen retrieval. After being blocked for an hour with 5% rabbit serum (Sigma–Aldrich), sections were incubated with a primary antibody (rat anti-collagen-II) (Santa Cruz Biotechnology, Dallas, TX) at 1:800 dilution overnight. Labeling was visualized with a rabbit anti-rat biotinylated IgG (Dako, Glostrup, Denmark) (1:600), streptavidin and biotin mix (Thermo Fisher Scientific, Scoresby, Australia) (1:700), and liquid diaminobenzidine (DAB+) (Dako) substrate for color development. Sections were then counterstained in haematoxylin (United Biosciences, QLD, Australia). Sections were observed by an Olympus BX41 microscope (Plympus, Notting Hill, Australia).

Micropatterning of CS-g-PNIPAAm

To prepare micropatterned templates, 0.5% (w/v) photoinitiator (2-hydroxy-1-(4-(hydroxyethoxy)phenyl)-2-methyl-1-propanone; Ir-gacur 2959) (CIBA Chemicals, Basel, Switzerland) was dissolved into 20% solution of poly(ethylene glycol)-dimethacrylate (MW 1000, PolyScience, Niles, IN) in PBS and vortexed. Then, 90 μL of the preheated solution was pipetted between an untreated glass and a 3-(trimethoxysilyl) propyl methacrylate (TMSPMA) (Sigma–Aldrich) coated glass slide separated by a 150 μm spacer. A photomask with parallel strips pattern was placed on top of the glass slide and exposed to 800 mW UV light (8 cm distance) for 120 s. After photocrosslinking, the glass slide was removed and washed gently with preheated PBS to remove unreacted solution. Unpatterned rectangular PEG-DMA hydrogels were prepared with the same method. The micropatterned and unpatterned PEG-DMA hydrogels were kept in PBS until use.

Then, 90 μL of aforementioned cell-laden CS-g-PNIPAAm solution (cell density: 1.0×10^7 cells/mL polymer solution, polymer concentration: 2.5 wt%) was placed on top of PEG-DMA micropatterned

template, gently pressed by a coverslip and was left in an incubator at 37 °C for 20 min to form gel. The coverslip was carefully taken off by sliding and any excess CS-g-PNIPAAm on PEG-DMA spacing was removed by sliding a sterile coverslip all over the micropatterned surface. Micropatterned cell-laden CS-g-PNIPAAm hydrogel within PEG-DMA micromolds (hereinafter microconstructs) were trans-ferred to a 6-well plate containing either preheated growth or chondrogenic medium and kept in a humidified incubator at 37 °C and 5% CO_2. Culturing media were replaced once every other day.

Live/Dead Cell Staining

The LIVE/DEAD® cytotoxicity/viability kit (Molecular Probes) was used to stain live and dead cells as per manufacturer's recommended protocol. A working solution of 0.5 μL/mL of calcein acetotoxymethyl ester (calcein AM) and 2 μL/mL of ethidium homodimer-1 (EthD-1) in PBS were prepared. Samples were washed with pre-warmed PBS, incubated in dye solution for 20 min, and washed three times with pre-warmed PBS. All the liquid was discarded and any entrapped liquid was absorbed by softly rubbing the hydrogel surface with a piece of tissue paper. As a result, the gel was made highly concentrated (semi-dried) to stabilize the structure of the thermosensitive hydrogel at room temperature and prevent its dissolution during handling. Embed-ded cells were observed under a fluorescence microscope (Nikon TE 2000, Tokyo, Japan) equipped with a temperature controlled chamber to keep the temperature at 37 °C. Samples were excited at 494 and 528 nm and emissions were read at 517 and 617 nm for live (green) and dead (red) cells, respectively.

Quantification of Cellular Alignment and Elongation

F-actin and nucleus were stained to quantify cellular alignment and elongation. For F-actin staining, cell-seeded gels were fixed in paraformaldehyde (4%) for 30 min. The cells were then permeabilized in a Triton X-100 solution (0.1% w/v) in PBS for 20 min and blocked in bovine serum albumin (BSA) (1% w/v) for 1 h. The samples were then incubated in a solution of 1:40 ratio of Alexa Fluor-594 phalloidin (Invitrogen, Carlsbad, CA) in BSA (0.1%) for 45 min at room temperature to stain actin filaments of the cell cytoskeleton. Samples were rinsed in PBS and counter-stained with 1 μL/mL of 4′,6-diamidino-2-phenylindole (DAPI) (Sigma–Aldrich) in PBS for 5 min in an incubator. Samples were washed with PBS and visualized using a Nikon TE 2000 fluorescence microscope (Japan), equipped with an environmental chamber. Cell elongation and alignment were quantified as previously demon-strated (Annabi et al., 2013; Aubin et al., 2010).

Using the built-in functions of the NIH ImageJ software, the best ellipse was fitted to the individual DAPI stained nuclei. The nuclear alignment was defined as the angle between the major axis of the fitted ellipse and the horizontal axis. The average orientation of all nuclei per sample was calculated, and all nuclear alignment angles were then normalized to it. Alignment angles were then grouped in 10° increments with respect to the average orientation. Cells with less than 20° of orientation were considered as aligned cells as previously described (Annabi et al., 2013). The cell elongation was also

described by shape index. The aspect ratio between the major and the minor elliptical axes of each individual cell nucleus was considered as shape index. Therefore, the shape index of a circle is one. The effects of channel width and culture time on cellular alignment and elongation were investigated by using micropatterned gels with a channel size of 50, 100, and 150 μm at different post-seeding time (1 and 5 days). For quantification, at least four images per sample and from three samples were used for each condition.

Multiphoton Microscopy

After 21 days of incubation in chondrogenic medium, micro-patterned cell-laden microconstructs were rinsed twice in preheated PBS. The excess liquid was extracted from the CS-g-PNIPAAm hydrogel using a piece of tissue paper to avoid hydrogel liquidation. The autofluorescence (AF) and second harmonic generation (SHG) signals were detected using a LaVision BioTec TriM Scope multiphoton microscope (Bielefeld, Germany) with two-photon excitation at 840 nm using a Ti:Sa laser (Coherent, Santa Clara, CA) and emission bandwidths of 470–550 nm and 410–430 nm for autofluorescence and SHG, respectively.

Statistical Analysis

All measurements were performed in triplicates unless otherwise stated. Data obtained from our experiments are represented as mean ± SD (standard deviation) or ±SE (standard error). Statistical significance was determined by application of Student's t-test. The differences were considered to be significant when $P < 0.05$.

Results and Discussion

Hydrogel Optimization for 3D Cell Encapsulation

CS-g-PNIPAAm hydrogels were first screened and optimized for 3D MSC culture and maintenance. A range of CS-g-PNIPAAm hydrogels with different grafting characteristics and therefore

Table I. Summary for the graft polymerization of NIPAAm onto chitosan.

Sample name	T_{rxn} (°C)[a]	GR (%)[b]	G' (pa)[c] at 37 °C
CSNI-1	60	130	18 ± 3
CSNI-2	25	212	101 ± 9

[−NH₂]:[CAN]:[NIPAAm] = 9:1:100.

−NH$_2$, chitosan free amino groups; CAN, initiator; and NIPAAm, monomer in feed. Chitosan was dissolved in 10% acetic acid. All reactions were carried out for 24 h.

[a]T_{rxn}: Reaction temperature.

[b]Grafting ratio (GR) was calculated as $(W_2 - W_1)/W_1 \times 100\%$, where W_1 and W_2 are the weights of initial chitosan loaded and PNIPAAm-grafted chitosan after soxhelet extraction, respectively.

[c]Measured by a cone and plate rheometer for 3.0 wt% of CS-g-PNIPAAm copolymers in PBS (pH = 7.4) at 1 rad/s. ($n = 3$, mean ± SD.)

different mechanical properties were prepared in our previous work (Mellati et al., 2014). Based on the solubility and mechanical properties (Mellati et al., 2014), we further selected the polymerization temperature as a control variable to synthesize two different CS-g-PNIPAAm polymers (CSNI-1 and CSNI-2) and evaluated the metabolic activity of encapsulated MSCs. Table I summarizes the details of the two synthesized polymers. CSNI-1 was polymerized at 60 °C. The grafting ratio, representing the number of PNIPAAm side chains grafted onto chitosan backbone, for CSNI-1 was 130% and storage modulus, a mechanical parameter for evaluating gel strength, was 18 ± 3 Pa at 37 °C. To produce CSNI-2 with higher mechanical properties (storage modulus of 101 ± 9 Pa), the reaction temperature was reduced to 25 °C and hence the grafting ratio increased to 212%. Figure 1a shows the metabolic activity of MSCs cultured in these two polymers measured by MTT assay. Cellular metabolic activity in CSNI-2 sample was significantly higher than CSNI-1. This higher metabolic activity might be attributed to the better mechanical properties of CSNI-2 that made it a better matrix for MSC encapsulation. It is well known that cells sense and respond to mechanical properties of their surrounding environment by translating them to chemical signals (Lutolf and Hubbell, 2005). Mechanical cues can consequently affect cell fate and behaviours such as viability,
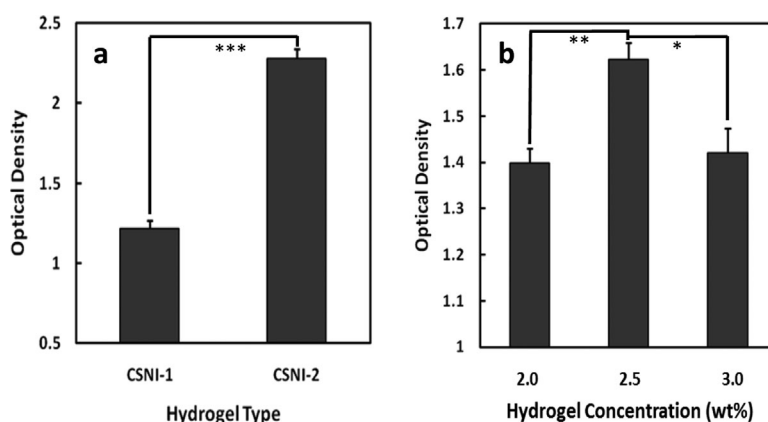
Figure 1. Optimisation of 3D cell culture conditions for MSCs. Absorbance of MTT after 7 days incubation at different (**a**) CS-g-PNIPAAm hydrogels (3.0 wt%) synthesized at different reaction temperatures which led to various grafting ratios and mechanical properties, and (**b**) CSNI-2 hydrogel concentrations. ($n = 3$, mean ± SE, *$P < 0.05$, **$P < 0.01$, ***$P < 0.001$.)

proliferation, differentiation, migration, and apoptosis (Guilak et al., 2009). Therefore, CSNI-2 sample was employed for all subsequent studies.

The influence of polymer concentration on cellular proliferation was studied at three different polymer concentrations (2.0, 2.5, and 3.0 wt%) of the selected sample CSNI-2. Figure 1b illustrates the metabolic activity of MSCs encapsulated in various hydrogels measured by MTT assay. Results revealed that the highest cellular proliferation was achieved in the hydrogel formed by using 2.5 wt% of polymer. Polymer concentration alters gel physical and mechanical properties which accordingly affects the cell behavior (Bae et al., 2011; Kim et al., 2010; Nichol et al., 2010). A low gel concentration results in weaker gels which cannot provide sufficient mechanical support to the encapsulated cells. A high gel concentration also generates a dense porous structure with smaller pore sizes and low interconnectivity (Dillon et al., 1998), which may hinder nutrient and oxygen delivery to cells and does not meet the cellular demands for self-renewal and migration. The CSNI-2 concentration of 2.5 wt% was thus chosen for the subsequent experiments.

MSC Differentiation in 3D Hydrogel

The CSNI-2 hydrogel with optimum concentration (2.5 wt%) was used for long-term (28 days) culture of MSCs in the presence of chondrogenic media to study the chondrogenic differentiation of the encapsulated cells. Cellular proliferation and production of cartilagous ECM (GAGs and collagen type II) were monitored during 28 days. In addition, constructs were histologically and immunohistologically examined at days 14 and 28 to confirm cartilage formation in the CSNI-2 hydrogel.

Cell proliferation was assessed by the Hoescht 33258 assay. The Hoescht assay results indicated that the cell number increased over culture time (Fig. 2a). Although, during the first 14 days, the proliferation rate was relatively slow [which might be due to cellular differentiation (Wang et al., 2005)], cells grew faster (almost twofold) during the following 2 weeks. The DMMB and hydroxyproline assays were employed to quantify GAGs and collagen deposition, respectively. The GAG level increased significantly from 0.8 µg/mg dry gel at day 7 to 4.8 µg/mg dry gel at day 28 (Fig. 2b). In addition, a sevenfold increase was observed in the total collagen accumulation during 28 days (Fig. 2c). GAGs and collagens are the main components of cartilagous tissues. Enhanced GAG and collagen deposition suggests the successful chondrogenic differentiation of MSCs within the 3D microenvironment provided by CSNI-2. The ECM deposition rate is equivalent (DeKosky et al., 2010) to or higher (Dai et al., 2010; Jin et al., 2010) than those of other biomaterials which have been used for cartilage tissue engineering. These results suggest that CSNI-2 gel could support 3D differentiation of MSCs to form cartilage tissue.

We further confirmed the cartilage tissue formation by histological and immunohistochemical staining of constructs as shown in Figure 3. Figure 3a and b shows low and high magnification micrographs of H&E staining. The dark spots represent cells while all other components including the deposited ECM and the polymeric hydrogel were stained in red. The polymer
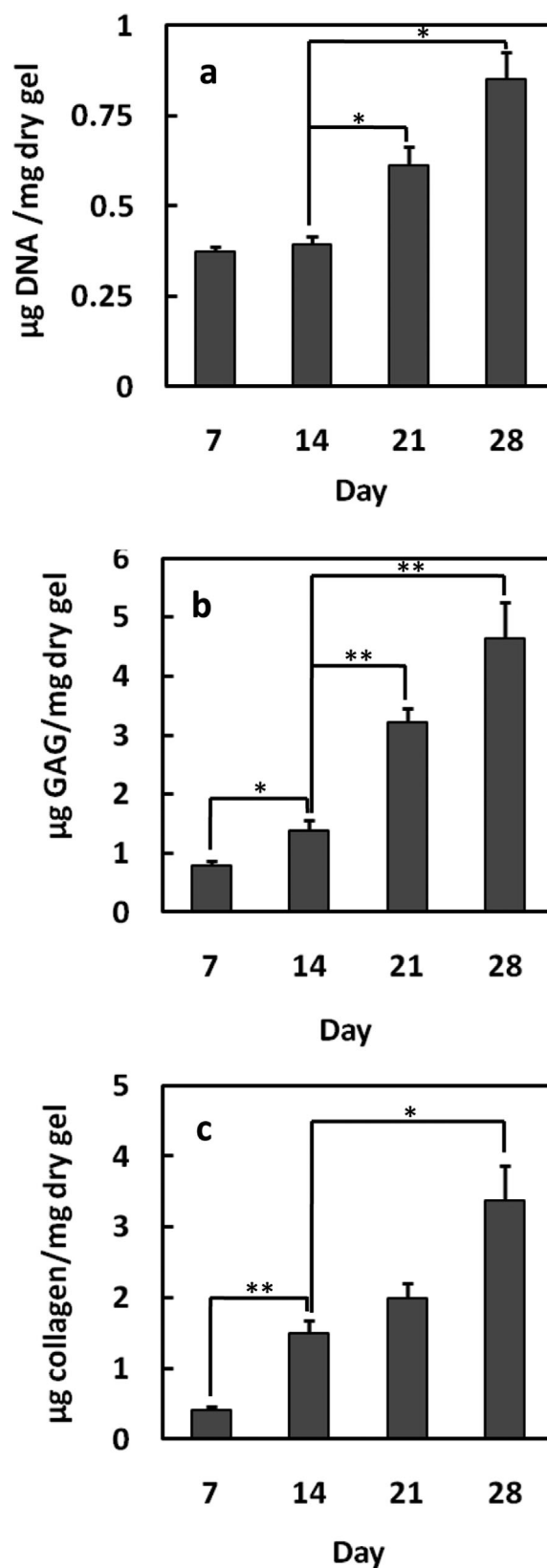
Figure 2. Quantification of (**a**) DNA, (**b**) GAG, and (**c**) total collagen in cell-seeded CSNI-2 over 4 weeks. All values were normalized by the dry weight of the hydrogel ($n = 3$, mean ± SE, $^*P < 0.05$, $^{**}P < 0.01$).
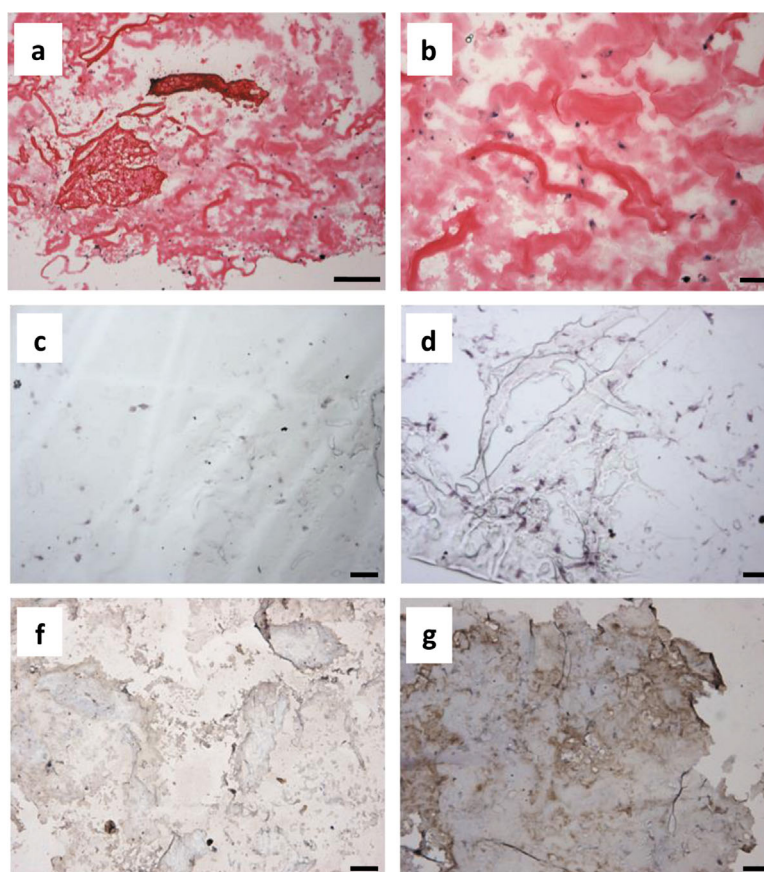
Figure 3. Histological and immunohistochemical staining of the cell-seeded hydrogels. (**a** and **b**) Sections were stained with H&E at (**a**) day 14 and (**b**) day 28; (**c** and **d**) sections were stained with Safranin O for GAGs after (**c**) 14 days and (**d**) 28 days of incubation; and (**f** and **g**) sections were immunohistochemically stained for collagen type II after (**e**) 14 days and (**f**) 28 days of incubation. (scale bar [a] = 200 μm, 4×; [b–g] = 50 μm, 10×.)

was also stained by Eosin because positively charged chitosan as a polymer component bound to the negatively charged dye. These images confirmed that cells were uniformly distributed in the structure. The hydrogel network surrounding the cells provided a 3D microenvironment that forced the cells to maintain a round shape, which is similar to the cellular morphology in the middle zone of the cartilage. Figure 3c and d represents safranin O-stained sections where the presence of GAGs within ECM can be distinguished by dark red color. Safranin-O did not bind the hydrogel but the background color of hydrogel had an influence on the staining color of the dye. The intensity of positively stained pericellular regions was increased from days 14 (Fig. 3c) to 28 (Fig. 3d). It confirmed the continuous GAG secretion by cells and formation of sulfated proteoglycan-rich ECM similar to native articular cartilage. Figure 3e and f shows the distribution of collagen type II, a cartilage-specific ECM component, by immunohisto-chemical staining. Positive collagen type II was stained in brown color. The darker stained regions around the cells at day 28 (Fig. 3f) than those for samples at day 14 (Fig. 3e) also confirmed the sustained collagen type II production over time as a key marker of chondrogenesis. Histological and immunohistochemical staining qualitatively verified the chondrogenic differentiation of MSCs encapsulated within CSNI-2 hydrogels. The level of GAG deposition

after 28 days of incubation looks similar to those reported in the literature for other hydrogels such as agarose and gelatin loaded with MSCs, after 90 days of culture in chondrogenic medium (Lin et al., 2014).

3D Cell-Laden Micropatterned Constructs

After optimization of the CS-g-PNIPAAm conditions for MSC encapsulation and its differentiation into chondrocytes, the hydrogel was used to create microconstructs in order to mimic the cellular shape and orientation within the superficial zone of native articular cartilage. PEG-DMA micromolds were fabricated using soft lithography and cell-laden thermoresponsive CSNI-2 were then thermally cast into the micromolds. Scheme 1b illustrates the fabrication process of microengineered cell-laden thermosensitive CSNI-2 hydrogel using microscale anisotropic PEG-DMA grooves as a micromold. Figure 4a presents a photograph of a micropatterned PEG-DMA on a TMSPMA glass slide. The overall dimension of the fabricated construct is 1.5 cm (L) × 1.4 cm (W) with a thickness of 150 μm. This thickness can be adjusted to mimic the thickness of the superficial zone which is around 200 μm. Figure 4b–d shows different PEG-DMA micropatterns with the same channel depth (150 μm) but three different groove widths
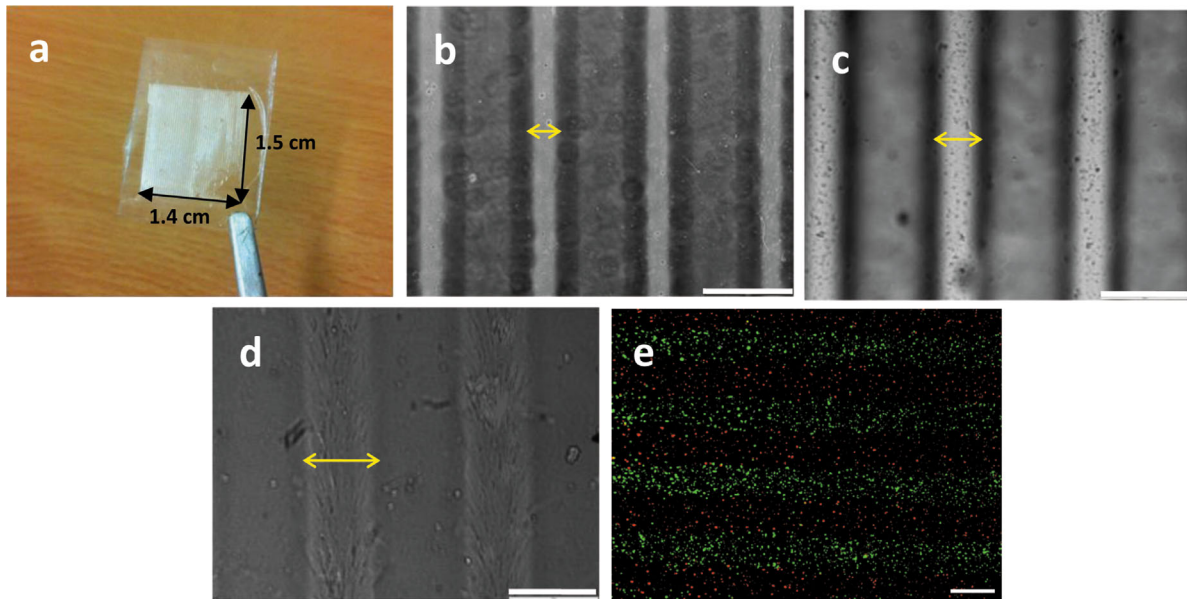
Figure 4. Images of micromolds and fabrication of micropatterned hydrogels. (**a**) Overview of a PEG-DMA micromold, with the dimensions of 1.4×1.5 cm². (**b–d**) Representative phase contrast images of PEG-DMA micromolds fabricated in different channel sizes: (**b**) 50 μm, (**c**) 100 μm, and (**d**) 150 μm. Yellow arrows show the channel width. (scale bars: 200 μm, 10×). (**e**) Fluorescent microscopic image of micropatterned hydrogel without cells. Green and red fluorescent beads were embedded in CS-g-PNIPAAm and PEG-DMA gels, respectively, before gelation (scale bar = 100 μm).

(50, 100, and 150 μm) at the same spacing between microgrooves (200 μm). The micrograph confirmed the high resolution of the soft lithography technique as well as the precise agreement between engineered constructs and the used photomasks. To ensure that CSNI-2 hydrogel had completely filled the PEG-DMA microchannels, different fluorescence beads were mixed with the two polymers and the construct was fabricated. PEG-DMA and CSNI-2 solutions were mixed with red and green fluorescent beads, respectively, prior to fabrication process. The construct was visualized under a fluorescence microscope equipped with an environmental chamber. Figure 4e demonstrates the distinct regions occupied with CSNI-2 and PEG-DMA.

MSCs were mixed with CSNI2 to fill the PEG-DMA micromolds. The constructs were then incubated for 5 days. The viability of encapsulated MSCs was evaluated using a live/dead assay. At day 1, viable cells were individually distributed with a round morphology within micropatterned hydrogel (Fig. 5a). At day 5, cells were connected to the neighbor cells and created a network-like assembly (Fig. 5b). A higher green intensity at day 5 in comparison to day 1 is related to the cellular proliferation and higher number of cells inside the hydrogel filling the microgrooves. The majority of cells remained viable while a few dead cells (stained in red) could be found at days 1 and 5.

The microconstructs were also stained with phalloidin and DAPI to visualize filamentous F-actin of the cytoskeleton and cell nuclei, respectively. Figure S1 (Supporting Information) displays a low magnification fluorescence image of cell-laden 3D CSNI-2 micropatterned hydrogel with multiple alternating parallel microconstructs at a width of 50 μm after 5 day incubation. It can be seen that cells were well organized within the microconstructs. At
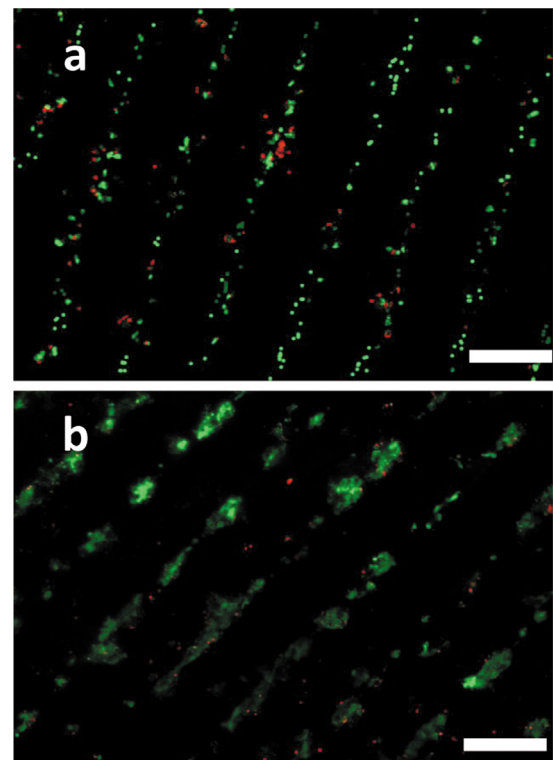
Figure 5. Live/dead cell staining of cell-laden micropatterned hydrogel (50 μm) after (**a**) 1 day and (**b**) 5 days of incubation. Green color indicates live cells and red spots represent dead cells. (scale bars = 200 μm, 4×.)
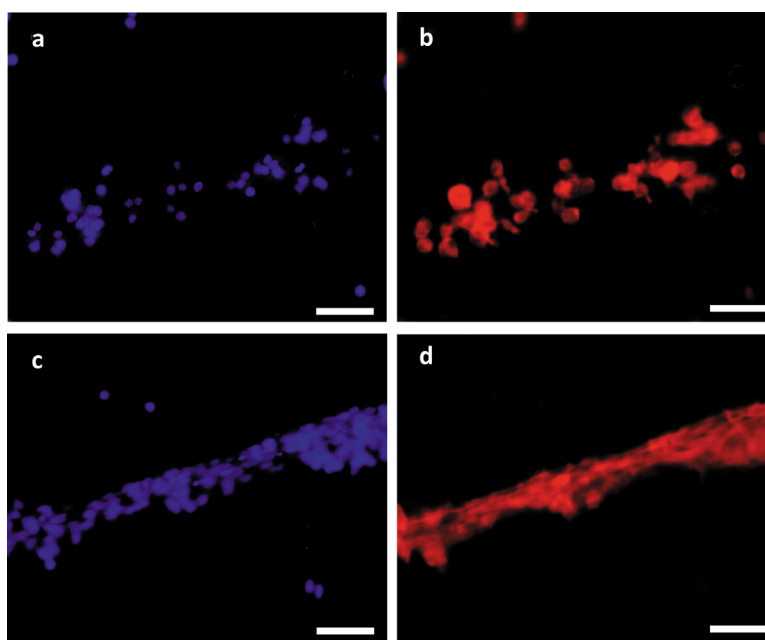
**Figure 6.** Fluorescence micrographs of cell alignment and elongation in microconstructs. Representative (**a** and **c**) DAPI and (**b** and **d**) F-actin-stained microconstruct (50 μm) of a cell-seeded hydrogel at days (**a** and **b**) 1 and (**c** and **d**) 5 of culture. (scale bars = 50 μm, 20×.)

some regions close to the top surface, cells were spread over the lateral ridges. A few cells were also left on top of the spacing walls during preparation of microconstructs because it was impossible to prevent all the cell-polymer solution from leaking out of the channels. While some parts in the microchannels might be peeled off during the staining and washing steps, the integral structure could be maintained without washing steps as will be shown later.

The images from cellular nucleus at days 1 and 5 are presented in Figure 6a and c, respectively. It can be seen that the individual cell nuclei were scattered in the hydrogel at day 1 in a round shape (Fig. 6a). More cell nuclei could be found at day 5 and the majority of them were in a stretched form (Fig. 6c). This confirms cellular proliferation inside the hydrogel within the grooves. Cells were also oriented along the horizontal axis of the microchannels. In addition, the cellular cytoskeleton was stretched along the main horizontal axis of the microgrooves at day 5 (Fig. 6d) in comparison to a round shape at day 1 (Fig. 6b), which demonstrates that cells have been re-oriented in the micropatterned hydrogels. Long stressed fibers were found to run in parallel according to the orientation of the cells. Aubin et al. (2010) suggested that cellular alignment was regulated by traction forces and matrix metalloproteinases (MMP)-mediated ECM remodeling. The traction forces were generated along the direction of the microgrooves due to the geometrical confinement which led to cell orientation (Nikkhah et al., 2012). These forces were also transferred to the neighboring cells through cell–cell junctions. Our results are in agreement with previous studies demonstrating that cells could be aligned and elongated when cultured on the surface of microgrooves (Charest et al., 2007; Hosseini et al., 2012; Thompson and Buettner, 2001) or encapsulated in patterned microconstructs (Aubin et al., 2010; Nikkhah et al., 2012).

Cell alignment was further quantified by the nuclear alignment angle which is defined as the orientation of the major axis of the nuclear shape by fitting in the best ellipse with respect to the horizontal axis of the microgrooves. Figure 7a–d represents the histogram of cell nuclear orientation in 10° increments within typical unpatterned and patterned microconstructs with a width of 150, 100, and 50 μm at day 5, respectively. The corresponding phalloidin and DAPI staining micrographs were also inserted as an internal panel in the histograms. The unpatterned histogram (Fig. 7a) shows that cell nuclei were randomly oriented in various directions. However, cell nuclei were stretched to some extent. This again confirmed that cells have been responsive to the supporting microenvironment with a high mechanical storage modulus. Histograms of 150, 100, and 50 μm wide microconstructs (Fig. 7b–d) revealed that more cells intended to have small nuclear angels with respect to the channel longitude axis by reducing the channel sizes, suggesting higher alignment at a smaller channel width. Figure 7e shows the percentage of the aligned cells in unpatterned and patterned gels with different widths. Cells were considered to be aligned when their nuclear angles were less than 20° with respect to the microchannel longitude axis represented by mean cell nuclear angles (Annabi et al., 2013). Figure 7e demonstrates that cells became more aligned over time in all patterned microconstructs, while there was no significant change in cell alignment in unpatterned constructs. The most significant increment over time was found in 100 μm microconstructs (from 25 ± 1% at day 1 to 74 ± 3% at day 5). At day 1, cells in 50 μm microgrooves were more aligned (45 ± 12%) in comparison with two other widths, while no significant difference could be seen between unpatterned, 150 and
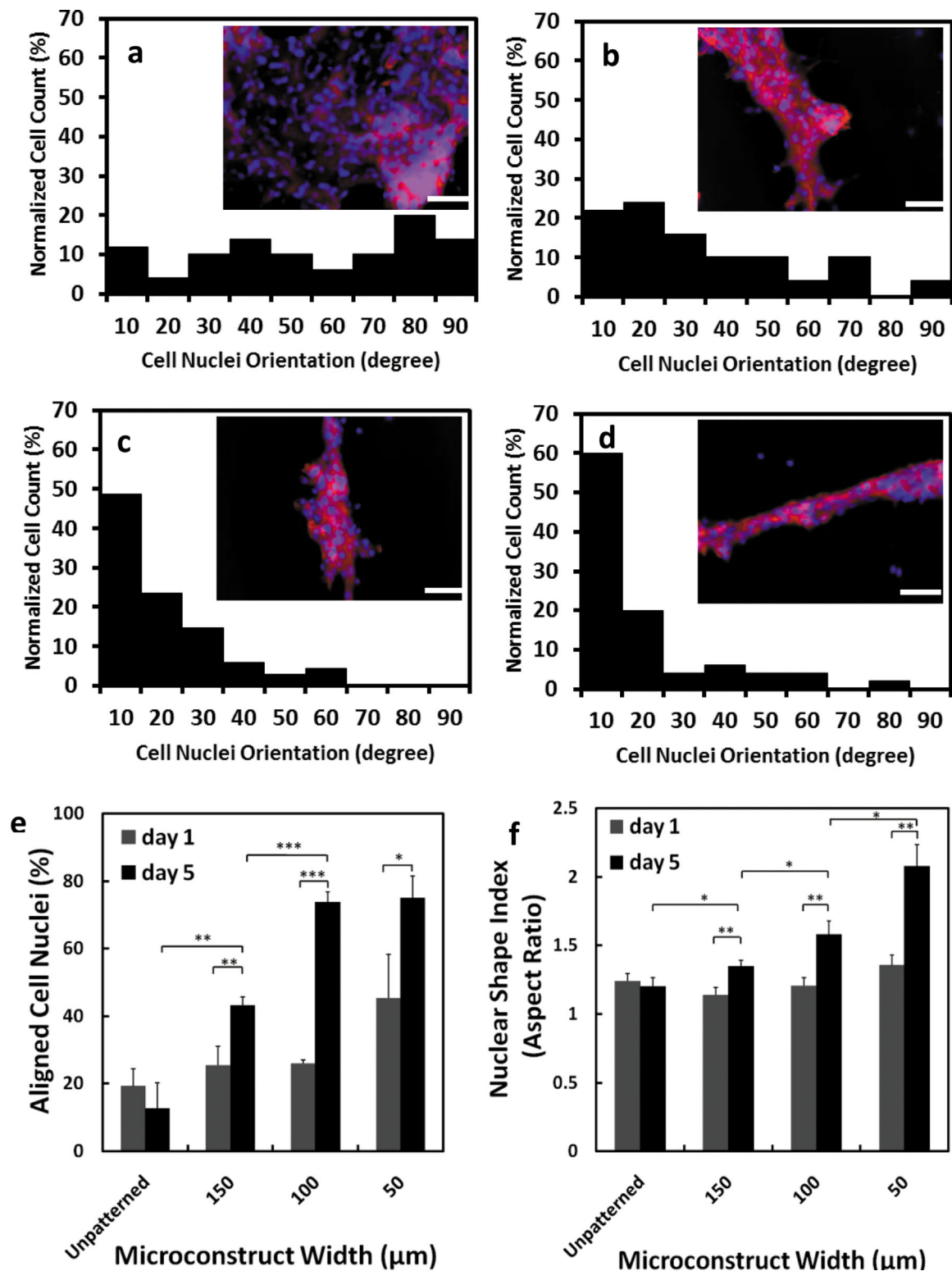
Figure 7. Quantification of cell alignment and elongation as a function of microconstruct width and incubation time. (a–d) Representative histograms of relative alignment in 10° increments on day 5 of culture in unpatterned and 150, 100, and 50 μm microchannel widths, respectively. Embedded images represent high magnification (20×) F-actin/DAPI stained microconstructs (scale bars [a–d] = 50 μm). (e) Mean percentage of aligned cell nuclei (within 20° of preferred nuclear orientation) in unpatternd and patterned gels at days 1 and 5. (f) Mean nuclear shape indices (aspect ratio) of unpatterned and patterned microconstructs at days 1 and 5. ($n = 3$, mean $\pm$ SD, $^*P < 0.05$, $^{**}P < 0.01$, $^{***}P < 0.001$).

Mellati et al.: Microengineered 3D Cell-Laden Thermoresponsive Hydrogels

227

Biotechnology and Bioengineering

100 μm micropatterns. At day 5, cells in 50 and 100 μm microconstructs (75 ± 6% and 74 ± 3%, respectively) were more aligned than those in 150 μm (43 ± 3%). Also, a significant increase was found for the percentage of cell alignment in all widths at day 5 in comparison with day 1, while no notable change was seen in unpatterned constructs. Interestingly, a similar percentage of aligned cells were found for 100 and 50 μm micropatterns at day 5. Jadin et al. (2007) quantified the chondrocyte organization by their angles to the nearest neighboring cell. They found that neighboring cells were arranged horizontally in the superficial zone with an averaged angle of 20° and vertically in the deep zone with an angle of 60°. In other regions of the cartilage, the angle was 32°, indicative of an isotropic organization. Our experiments suggested that cells encapsulated within 50–100 μm microgrooves were aligned in the pattern similar to the superficial zone and in gaps at 150 μm or wider were more likely to form the middle zone.

Cell elongation was quantitatively studied by estimating the cell nuclear shape index (CNSI). The CNSI, the ratio of the major to the minor axes of the best fit ellipse from individual cell nucleus, was employed as the shape index. Figure 7f shows the results of CNSIs in the unpatterned and patterned microconstructs with a width of 150, 100, and 50 μm at days 1 and 5. At day 1, there was no significant difference between CNSI in different groups including unpatterned and patterned hydrogels. The aspect ratio was close to 1 for all groups suggesting an almost round shape of cell nuclei. The CNSI did not change at day 5 in unpatterned gels (1.20 ± 0.07) in comparison with day 1 (1.24 ± 0.06). In contrast, within all patterned groups, CNSI at day 5 were greater than the values for the same group at day 1 ($P < 0.01$). The change became more significant by decreasing the microconstruct width. At day 5, the shape indices were significantly different ($P < 0.05$) between the unpatterned and patterned groups. The highest aspect ratio of 2.07 ± 0.16 was found for cells in the 50 μm micropatterns. These results suggest that cells become more elongated in the more narrow microgrooves and the extent of elongation can be adjusted by controlling the widths of the microgrooves. This is in agreement with previous studies (Annabi et al., 2013; Aubin et al., 2010).

Cell alignment and elongation studies confirmed the successful cellular organization similar to native articular cartilage. This organization is vital for the tissue functionality, homeostasis (Jadin et al., 2005), cell regulation through direct cell–cell contact and paracrine or autocrine factors, and determination of the zone-specific characteristics (Peng et al., 2014). Cellular organization has also a great impact on the local solid and fluid environment in which the cells reside, when the cells are exposed to external mechanical or chemical stimuli (Jadin et al., 2007). Among three zones, the superficial zone is the most important. Superficial zone chondrocytes modulate the surface mechanical properties of engineered cartilage (Peng et al., 2014). The flattened geometry of chondrocytes encourages the superficial zone phenotype (McNary et al., 2014). In addition, it has been demonstrated that the changes in cellular arrangement at the superficial zone of the articular cartilage arose at the onset of osteoarthritis (Becerra et al., 2010).

The cell-laden microconstructs were further incubated in the chondrogenic medium for 21 days and visualized under a multiphoton microscope for AF and SHG signals. Some cellular components and biomaterials are detectable under the multiphoton microscope due to their AF signals, including some cell contents such as nicotinamide adenine dinucleotide (NADH) coenzymes (Schenke-Layland et al., 2006), and cell debris (Schenke-Layland et al., 2003) as well as some biomaterials used as scaffolds in tissue engineering (Heydarkhan-Hagvall et al., 2008; Lee et al., 2006) including chitosan (Chen et al., 2010). As the multiphoton microscope can detect autofluorescence signals, therefore, microconstructs do not need any staining and washing steps and solution changes can be avoided before imaging to prevent structural damage. An integrated architecture of AF signal (red) in Figure 8a confirmed that the structure of microconstructs was well preserved after 21 day incubation. Collagen in ECM can also be distinguishable from their SHG signals. Collagen is the strong source of second harmonics in animal tissues due to its unusual noncentrosymmetric structure and high degree of crystallinity (Cox and Kable, 2006). SHG signals of collagen (green) were observed as shown in Figure 8b. The detectable collagen signals denoted that MSCs were differentiating (Chen et al., 2010). Collagen was
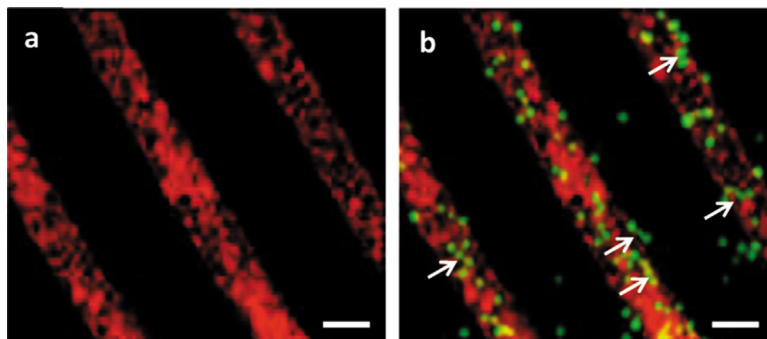
Figure 8. Multiphoton microscopy image of micropatterned cell-laden hydrogel after 21 days' incubation. (**a**) Autofluorescence (AF) of cell-laden CS-g-PNIPAAm gel. (**b**) Overlay of AF (red) and second harmonic generation signals (green), indicating collagens in extracellular matrix. White arrows indicate combined collagens from different cells. (scale bars = 100 μm, 10×.)

presented as a round shape, surrounding the individual cells. At some regions indicated by white arrows, collagen was aligned along the horizontal axis. The reason for the scattered collagen distribution might be due to the low cell density within the hydrogel constructs. As described earlier in DNA quantification, the cell number did not increase up to day 14, and the cells started to proliferate after 14 days (Fig. 2a). It is expected that after culturing in the chondrogenic medium for a longer time, collagen will be more integrated and aligned.

Images of safranin O histologically and collagen II immunohistologically stained microconstructs (cultured in the chondrogenic medium for 2 weeks) are presented in Figure S2 (Supporting Information). Although it was difficult to visualize the positive stains due to the high thickness of the microconstructs under the phase contrast microscopy, positive stains could be observed at the edges and broken regions of the gel (Fig. S2a, Supporting Information). Collagen type II-positive components were not distinguishable by immunostaining within the micropatterns due to the dark background of the thick gel (Fig. S2b, Supporting Information).

In our future study, the micropatterned and unpatterned layers will be stacked to form an integrated tissue engineered construct. Scheme S1 (Supporting Information) illustrates this concept. Furthermore, more detailed characterization of the engineered articular cartilage will be required, such as zone-specific proteins including superficial zone protein (SZP) for evaluating differentiation of MSCs to chondrocytes of zonal phenotype, and collagen type I staining to confirm that the engineered tissue is a hyaline cartilage and no fibrocartilage is formed.

Conclusions

MSCs were incorporated in CS-g-PNIPAAm (CSNI-1 and CSNI-2) as a thermosensitive hydrogel and cells proliferated faster in the CSNI-2 with a mechanically strong structure than in the CSNI-1. By incubating MSCs in the thermosensitive hydrogel in a chondrogenic medium for over 28 days, cartilaginous tissue formation was confirmed by biochemical, histochemical, and immunohistochemical assays. To control cell orientation and mimic the structure of native cartilage, the cell-laden thermoresponsive hydrogel was further micropatterned using PEG-DMA stamps by simply incubation at 37 °C without UV radiation and photoinitiators. Cells were aligned and elongated in the narrow microchannel gaps, suggesting that the microfabrication method can be exploited for 3D cell orientation and elongation to mimic the cell shape and organization in the superficial zone of native cartilages. However, cells in the wide microchannel as unpatterned microstructures served to resemble the middle zone of articular cartilage. Recreating an integrated macroscale tissue by stacking the microconstructs remains to be addressed in our future research. Our results suggest that micropatterning of 3D cell-laden CS-g-PNIPAAm (CSNI-2) hydrogel is a promising method for controlling cell shape and morphology in bi-zonal cartilage tissue engineering.

References

Albrecht DR, Tsang VL, Sah RL, Bhatia SN. 2005. Photo-and electropatterning of hydrogel-encapsulated living cell arrays. Lab Chip 5(1):111–118.

Annabi N, Tamayol A, Uquillas JA, Akbari M, Bertassoni LE, Cha C, Camci-Unal G, Dokmeci MR, Peppas NA, Khademhosseini A. 2014. 25th Anniversary article: Rational design and applications of hydrogels in regenerative medicine. Adv Mater 26(1):85–124.

Annabi N, Tsang K, Mithieux SM, Nikkhah M, Ameri A, Khademhosseini A, Weiss AS. 2013. Highly elastic micropatterned hydrogel for engineering functional cardiac tissue. Adv Funct Mater 23(39):4950–4959.

Aubin H, Nichol JW, Hutson CB, Bae H, Sieminski AL, Cropek DM, Akhyari P, Khademhosseini A. 2010. Directed 3D cell alignment and elongation in microengineered hydrogels. Biomaterials 31(27):6941–6951.

Bae H, Ahari AF, Shin H, Nichol JW, Hutson CB, Masaeli M, Kim S-H, Aubin H, Yamanlar S, Khademhosseini A. 2011. Cell-laden microengineered pullulan methacrylate hydrogels promote cell proliferation and 3D cluster formation. Soft Matter 7(5):1903–1911.

Becerra J, Andrades JA, Guerado E, Zamora-Navas P, López-Puertas JM, Reddi AH. 2010. Articular cartilage: Structure and regeneration. Tissue Eng Part B Rev 16(6):617–627.

Bryant SJ, Anseth KS. 2003. Controlling the spatial distribution of ECM components in degradable PEG hydrogels for tissue engineering cartilage. J Biomed Mater Res A 64(1):70–79.

Charest JL, García AJ, King WP. 2007. Myoblast alignment and differentiation on cell culture substrates with microscale topography and model chemistries. Biomaterials 28(13):2202–2210.

Chen T, Hilton MJ, Brown EB, Zuscik MJ, Awad HA. 2013. Engineering superficial zone features in tissue engineered cartilage. Biotechnol Bioeng 110(5):1476–1486.

Chen W-L, Huang C-H, Chiou L-L, Chen T-H, Huang Y-Y, Jiang C-C, Lee H-S, Dong C-Y. 2010. Multiphoton imaging and quantitative analysis of collagen production by chondrogenic human mesenchymal stem cells cultured in chitosan scaffold. Tissue Eng Part C Methods 16(5):913–920.

Cho JH, Kim S-H, Park KD, Jung MC, Yang WI, Han SW, Noh JY, Lee JW. 2004. Chondrogenic differentiation of human mesenchymal stem cells using a thermosensitive poly (N-isopropylacrylamide) and water-soluble chitosan copolymer. Biomaterials 25(26):5743–5751.

Chung R, Cool JC, Scherer MA, Foster BK, Xian CJ. 2006. Roles of neutrophil-mediated inflammatory response in the bony repair of injured growth plate cartilage in young rats. J Leukoc Biol 80(6):1272–1280.

Coates EE, Fisher JP. 2014. Engineering superficial zone chondrocytes from mesenchymal stem cells. Tissue Eng Part C Methods 20(8):630–640.

Cox G, Kable E. 2006. Second-harmonic imaging of collagen. Methods Mol Biol 319:15–35.

Dai W, Kawazoe N, Lin X, Dong J, Chen G. 2010. The influence of structural design of PLGA/collagen hybrid scaffolds in cartilage tissue engineering. Biomaterials 31(8):2141–2152.

DeKosky BJ, Dormer NH, Ingavle GC, Roatch CH, Lomakin J, Detamore MS, Gehrke SH. 2010. Hierarchically designed agarose and poly (ethylene glycol) interpenetrating network hydrogels for cartilage tissue engineering. Tissue Eng Part C Methods 16(6):1533–1542.

Di Martino A, Sittinger M, Risbud MV. 2005. Chitosan: A versatile biopolymer for orthopaedic tissue engineering. Biomaterials 26(30):5983–5990.

Dillon GP, Xiaojun Y, Sridharan A, Ranieri JP, Bellamkonda RV. 1998. The influence of physical structure and charge on neurite extension in a 3D hydrogel scaffold. J Biomater Sci Polym Ed 9(10):1049–1069.

Erisken C, Kalyon DM, Wang H. 2008. Functionally graded electrospun polycaprolactone and β-tricalcium phosphate nanocomposites for tissue engineering applications. Biomaterials 29(30):4065–4073.

Fedorovich NE, Alblas J, Wijin JR, Hennink WE, Verbout AJ, Dhert WJA. 2007. Hydrogels as extracellular matrices for skeletal tissue engineering: State-of-the-Art and novel application in organ printing. Tissue Eng 13(8):1905–1925.

Francis Suh JK, Matthew HWT. 2000. Application of chitosan-based polysaccharide biomaterials in cartilage tissue engineering: A review. Biomaterials 21(24):2589–2598.

Guilak F, Cohen DM, Estes BT, Gimble JM, Liedtke W, Chen CS. 2009. Control of stem cell fate by physical interactions with the extracellular matrix. Cell Stem Cell 5(1):17–26.

Heydarkhan-Hagvall S, Schenke-Layland K, Dhanasopon AP, Rofail F, Smith H, Wu BM, Shemin R, Beygui RE, MacLellan WR. 2008. Three-dimensional electrospun ECM-based hybrid scaffolds for cardiovascular tissue engineering. Biomaterials 29(19):2907–2914.

Hoemann CD. 2004. Molecular and biochemical assays of cartilage components. Methods Mol Med 101:127–156.

Hosseini V, Ahadian S, Ostrovidov S, Camci-Unal G, Chen S, Kaji H, Ramalingam M, Khademhosseini A. 2012. Engineered contractile skeletal muscle tissue on a microgrooved methacrylated gelatin substrate. Tissue Eng Part A 18(23–24):2453–2465.

Hunziker EB. 2002. Articular cartilage repair: Basic science and clinical progress. A review of the current status and prospects. Osteoarthr Cartil 10(6):432–463.

Hunziker EB, Quinn TM, Häuselmann HJ. 2002. Quantitative structural organization of normal adult human articular cartilage. Osteoarthr Cartil 10(7):564–572.

Hwang NS, Varghese S, Elisseeff J. 2007a. Cartilage tissue engineering. Methods Mol Biol 407:351–373.

Hwang NS, Varghese S, Lee HJ, Theprungsirikul P, Canver A, Sharma B, Elisseeff J. 2007b. Response of zonal chondrocytes to extracellular matrix-hydrogels. FEBS Lett 581(22):4172–4178.

Jadin KD, Bae WC, Schumacher BL, Sah RL. 2007. Three-dimensional (3-D) imaging of chondrocytes in articular cartilage: Growth-associated changes in cell organization. Biomaterials 28(2):230–239.

Jadin KD, Wong BL, Bae WC, Li KW, Williamson AK, Schumacher BL, Price JH, Sah RL. 2005. Depth-varying density and organization of chondrocytes in immature and mature bovine articular cartilage assessed by 3D imaging and analysis. J Histochem Cytochem 53(9):1109–1119.

Jin R, Moreira Teixeira L, Dijkstra P, van Blitterswijk C, Karperien M, Feijen J. 2010. Enzymatically-crosslinked injectable hydrogels based on biomimetic dextran–hyaluronic acid conjugates for cartilage tissue engineering. Biomaterials 31(11):3103–3113.

Johnstone B, Alini M, Cucchiarini M, Dodge GR, Eglin D, Guilak F, Madry H, Mata A, Mauck RL, Semino CE. 2013. Tissue engineering for articular cartilage repair-the state of the art. Eur Cell Mater 25:248–267.

Keeney M, Lai JH, Yang F. 2011. Recent progress in cartilage tissue engineering. Curr Opin Biotechnol 22(5):734–740.

Kim I-Y, Seo S-J, Moon H-S, Yoo M-K, Park I-Y, Kim B-C, Cho C-S. 2008. Chitosan and its derivatives for tissue engineering applications. Biotechnol Adv 26(1):1–21.

Kim M, Lee JY, Jones CN, Revzin A, Tae G. 2010. Heparin-based hydrogel as a matrix for encapsulation and cultivation of primary hepatocytes. Biomaterials 31(13):3596–3603.

Kim T-K, Sharma B, Williams C, Ruffner M, Malik A, McFarland E, Elisseeff J. 2003. Experimental model for cartilage tissue engineering to regenerate the zonal organization of articular cartilage. Osteoarthr Cartil 11(9):653–664.

Klein T, Schumacher B, Schmidt T, Li K, Voegtline M, Masuda K, Thonar E, Sah R. 2003. Tissue engineering of stratified articular cartilage from chondrocyte subpopulations. Osteoarthr Cartil 11(8):595–602.

Klein TJ, Rizzi SC, Schrobback K, Reichert JC, Jeon JE, Crawford RW, Hutmacher DW. 2010. Long-term effects of hydrogel properties on human chondrocyte behavior. Soft Matter 6(20):5175–5183.

Kock LM, Ito K, van Donkelaar CC. 2013. Sliding indentation enhances collagen content and depth-dependent matrix distribution in tissue-engineered cartilage constructs. Tissue Eng Part A 19(17–18):1949–1959.

Lanza R, Longer R, Vacanti J. 2007. Principles of tissue engineering. London: Academic Press. p 1825.

Lee CS, Gleghorn JP, Won Choi N, Cabodi M, Stroock AD, Bonassar LJ. 2007. Integration of layered chondrocyte-seeded alginate hydrogel scaffolds. Biomaterials 28(19):2987–2993.

Lee H-S, Teng S-W, Chen H-C, Lo W, Sun Y, Lin T-Y, Chiou L-L, Jiang C-C, Dong C-Y. 2006. Imaging human bone marrow stem cell morphogenesis in polyglycolic acid scaffold by multiphoton microscopy. Tissue Eng 12(10):2835–2841.

Lin H, Cheng AW-M, Alexander PG, Beck AM, Tuan RS. 2014. Cartilage tissue engineering application of injectable gelatin hydrogel with In situ visible-Light-Activated gelation capability in both air and aqueous solution. Tissue Eng Part A 20(17–18):2402–2411.

Liu VA, Bhatia SN. 2002. Three-dimensional photopatterning of hydrogels containing living cells. Biomed Microd 4(4):257–266.

Lutolf MP, Hubbell JA. 2005. Synthetic biomaterials as instructive extracellular microenvironments for morphogenesis in tissue engineering. Nat Biotech 23(1):47–55.

Mansour JM. 2003. Biomechanics of cartilage. In: Oatis CA, editor. Kinesiology: The mechanics and pathomechanics of human movement. Baltimore, MD: Lippincott Williams and Wilkins. p 66–79.

Marsano A, Wendt D, Quinn T, Sims T, Farhadi J, Jakob M, Heberer M, Martin I. 2006. Bi-zonal cartilaginous tissues engineered in a rotary cell culture system. Biorheology 43(3):553–560.

McCullen SD, Autefage H, Callanan A, Gentleman E, Stevens MM. 2012. Anisotropic fibrous scaffolds for articular cartilage regeneration. Tissue Eng Part A 18(19–20):2073–2083.

McNary SM, Athanasiou KA, Reddi AH. 2014. Transforming growth factor β-induced superficial zone protein accumulation in the surface zone of articular cartilage is dependent on the cytoskeleton. Tissue Eng Part A 20(5–6):921–929.

Mellati A, Dai S, Bi J, Jin B, Zhang H. 2014. A biodegradable thermosensitive hydrogel with tuneable properties for mimicking three-dimensional microenvironments of stem cells. RSC Adv 4:63951–63961.

Newman AP. 1998. Articular cartilage repair. A J Sports Med 26(2):309–324.

Ng KW, Wang CCB, Mauck RL, Kelly TAN, Chahine NO, Costa KD, Ateshian GA, Hung CT. 2005. A layered agarose approach to fabricate depth-dependent inhomogeneity in chondrocyte-seeded constructs. J Orthop Res 23(1):134–141.

Nguyen LH, Kudva AK, Saxena NS, Roy K. 2011. Engineering articular cartilage with spatially-varying matrix composition and mechanical properties from a single stem cell population using a multi-layered hydrogel. Biomaterials 32(29):6946–6952.

Nichol JW, Koshy ST, Bae H, Hwang CM, Yamanlar S, Khademhosseini A. 2010. Cell-laden microengineered gelatin methacrylate hydrogels. Biomaterials 31(21):5536–5544.

Nikkhah M, Eshak N, Zorlutuna P, Annabi N, Castello M, Kim K, Dolatshahi-Pirouz A, Edalat F, Bae H, Yang Y, Khademhosseini A. 2012. Directed endothelial cell morphogenesis in micropatterned gelatin methacrylate hydrogels. Biomaterials 33(35):9009–9018.

Peng G, McNary SM, Athanasiou KA, Reddi AH. 2014. Surface zone articular chondrocytes modulate the bulk and surface mechanical properties of the tissue-engineered cartilage. Tissue Eng Part A 20(23–24):3332–3341.

Poole AR, Kojima T, Yasuda T, Mwale F, Kobayashi M, Laverty S. 2001. Composition and structure of articular cartilage: A template for tissue repair. Clin Orthop Relat Res 391:S26–S33.

Ren Z, Wang Y, Ma S, Duan S, Yang X, Gao P, Zhang X, Cai Q. 2015. Effective bone regeneration using thermosensitive poly (N-isopropylacrylamide) grafted gelatin as injectable carrier for bone mesenchymal stem cells. ACS Appl Mater Interfaces 7(34):19006–19015.

Schenke-Layland K, Riemann I, Damour O, Stock UA, König K. 2006. Two-photon microscopes and in vivo multiphoton tomographs—Powerful diagnostic tools for tissue engineering and drug delivery. Adv Drug Deliv Rev 58(7):878–896.

Schenke-Layland K, Vasilevski O, Opitz F, König K, Riemann I, Halbhuber K, Wahlers T, Stock U. 2003. Impact of decellularization of xenogeneic tissue on extracellular matrix integrity for tissue engineering of heart valves. J Struct Biol 143(3):201–208.

Schrobback K, Malda J, Crawford RW, Upton Z, Leavesley DI, Klein TJ. 2012. Effects of oxygen on zonal marker expression in human articular chondrocytes. Tissue Eng Part A 18(9–10):920–933.

Sharma B, Elisseeff JH. 2004. Engineering structurally organized cartilage and bone tissues. Ann Biomed Eng 32(1):148–159.

Sharma B, Williams CG, Kim TK, Sun D, Malik A, Khan M, Leong K, Elisseeff JH. 2007. Designing zonal organization into tissue-engineered cartilage. Tissue Eng 13(2):405–414.

Spiller KL, Maher SA, Lowman AM. 2011. Hydrogels for the repair of articular cartilage defects. Tissue Eng Part B Rev 17(4):281–299.

Spitters TW, Leijten JC, Deus FD, Costa IB, van Apeldoorn AA, van Blitterswijk CA, Karperien M. 2013. A dual flow bioreactor with controlled mechanical stimulation for cartilage tissue engineering. Tissue Eng Part C Methods 19(10):774–783.

Spitters TW, Mota CM, Uzoechi SC, Slowinska B, Martens D, Moroni L, Karperien M. 2014. Glucose gradients influence zonal matrix deposition in 3D cartilage constructs. Tissue Eng Part A 20(23–24):3720–3728.

Steele J, McCullen S, Callanan A, Autefage H, Accardi M, Dini D, Stevens M. 2014. Combinatorial scaffold morphologies for zonal articular cartilage engineering. Acta Biomater 10(5):2065–2075.

Temenoff JS, Mikos AG. 2000. Review: Tissue engineering for regeneration of articular cartilage. Biomaterials 21(5):431–440.

Thompson DM, Buettner HM. 2001. Schwann cell response to micropatterned laminin surfaces. Tissue Eng 7(3):247–265.

Thorpe SD, Nagel T, Carroll SF, Kelly DJ. 2013. Modulating gradients in regulatory signals within mesenchymal stem cell seeded hydrogels: A novel strategy to engineer zonal articular cartilage. PloS ONE 8(4):e60764.

Walker KJ, Madihally SV. 2014. Anisotropic temperature sensitive chitosan-based injectable hydrogels mimicking cartilage matrix. J Biomed Mater Res B Appl Biomater 103(6):1149–1160.

Wang Y, Kim U-J, Blasioli DJ, Kim H-J, Kaplan DL. 2005. In vitro cartilage tissue engineering with 3D porous aqueous-derived silk scaffolds and mesenchymal stem cells. Biomaterials 26(34):7082–7094.

Wise JK, Yarin AL, Megaridis CM, Cho M. 2008. Chondrogenic differentiation of human mesenchymal stem cells on oriented nanofibrous scaffolds: Engineering the superficial zone of articular cartilage. Tissue Eng Part A 15(4):913–921.

Woodfield T, Blitterswijk CV, Wijn JD, Sims T, Hollander A, Riesle J. 2005. Polymer scaffolds fabricated with pore-size gradients as a model for studying the zonal organization within tissue-engineered cartilage constructs. Tissue Eng 11(9–10):1297–1311.

Xu Y, Li Z, Li X, Fan Z, Liu Z, Xie X, Guan J. 2015. Regulating myogenic differentiation of mesenchymal stem cells using thermosensitive hydrogels. Acta Biomater 26:23–33.

Supporting Information

Additional supporting information may be found in the online version of this article at the publisher's web-site.